Electronic Supplementary Information (ESI)

Gas-liquid interface-mediated room-temperature synthesis of "clean" PdNiP alloy networks with high catalytic activity for ethanol oxidation

Rongfang Wang[1, *], Yuanyuan Ma[1], Hui Wang[1], Julian Key[2], and Shan Ji[2]

1 Key Laboratory of Eco-Environment-Related Polymer Materials, Ministry of Education of China, College of Chemistry and Chemical Engineering, Northwest Normal University, Lanzhou 730070, China
2 South African Institute for Advanced Materials Chemistry, University of the Western Cape, Private Bag X17, Bellville, Cape Town 7535, South Africa

Experimental

Synthesis

All reagents were of analytic grade and ultrapure water was used throughout the experiments. To prepare PdNiP nanoparticle alloy networks (Sample PdNiP-1 NN), we first made three solutions: (1) 270 mg of $NiCl_2 \cdot 6H_2O$ and 200 mg of $NaH_2PO_2 \cdot H_2O$ were dissolved in 30 mL water bubbled continuously with N_2, (2) 95 mg of $NaBH_4$ was dissolved in 20 mL water and the solution was transferred to a constant funnel, and (3) 20 mg of $PdCl_2$ was dissolved in 10 mL water and adjusted to ~Ph 7.5 using 6 mol L^{-1} NaOH solution with vigorous stirring. Solution (2) was added dropwise into solution (1) under the stirring conditions and bubbled with N_2. Then, solution (3) was rapidly added to the mixture and stirred vigorously for another 4 h with continuously bubbled N_2. In the reaction scheme, $PdCl_2$, $NiCl_2$, and

R.F. Wang (*): wrf38745779@126.com, Tel./fax: +86-931-7971533

$NaH_2PO_2 \cdot H_2O$ were reduced to produce PdNiP and $NaBH_4$ via the following reactions:

$$Pd^{2+} \xrightarrow{NaBH_4} Pd$$

$$Ni^{2+} \xrightarrow{NaBH_4} Ni$$

$$H_2PO_2^- \xrightarrow{NaBH_4} P+H_2O$$

$$xPd+yNi+zP \longrightarrow Pd_xNi_yP_z$$

The resultant precipitate was collected by filtration, washed with 6 mol L^{-1} ammonia solution, then washed with deionized water several times and stored in ethanol solution. To obtain alloy networks of different composition, we altered the precursor ratio as listed below in Table S1.

Table S1. Synthesis conditions, the ratio of different precursors, composition and BET surface area of obtained samples.

Sample	Bubbled N2	Initial ratio Pd:Ni:P	Actual ratio Pd:Ni:P
PdNiP-1 NN	√	1:10:18	1:5.2:11
PdNiP-2	√	1:10:14	1:5:8
PdNiP-3	√	1:10:11	1:5.2:5.5
PdNi NN	√	1:10	1:6
PdNiP GA	√	1:10:14	1:5.1:8.3

Characterization

XRD patterns were recorded on a Shimadzu XD–3A (Japan) using filtered Cu-Kα radiation (λ = 0.15418 nm) generated at 40 kV and 30 mA. Scans for 2θ values were

recorded at 4° min^{-1}. Scanning electron microscopy (SEM) images were obtained using a Carl Zeiss Ultra Plus. Transmission electron microscopy (TEM) high angle annular dark field scanning transmission electron microscopy (STEM) images and selected area electron diffraction (SAED) patterns of the catalysts were obtained using a JEOL (JEM-2000 FX) microscope operating at 200 kV. Line-scan energy dispersive spectroscopy (EDS) in the STEM mode was used for elemental composition analysis. The average chemical compositions of the catalysts were obtained using an IRIS advantage inductively coupled plasma atomic emission spectroscopy (ICP-AES) system (Thermo, America). The specific surface area was determined by Brunauer - Emmett-Teller (BET) method on Quantachrome Autosorb-1 volumetric analyzer (America). X-ray photoelectron spectra (XPS) was acquired with a VGEscalab210 spectrometer fitted with Mg 300 W X-ray source.

Electrochemical measurements

Electrochemical measurements were carried out using an electrochemical work station CHI 650D. A common three-electrode electrochemical cell was used for the measurements. The counter and reference electrodes were a platinum wire and a Hg/HgO (1 mol L^{-1} KOH) electrode respectively. The working electrode was prepared on a 5-mm diameter glassy carbon disk, were 2 mg of catalyst was dispersed ultrasonically in 0.4 mL Nafion/ethanol (0.25% Nafion) solution for 15 min, and 8 μL was pipetted and air dried on the glassy carbon surface. For CO stripping tests, CO was first adsorbed on the working electrode by bubbling CO through the electrolyte

for 5 min, followed by its transfer to a cell containing nitrogen-purged 1.0 mol L^{-1} KOH solution.

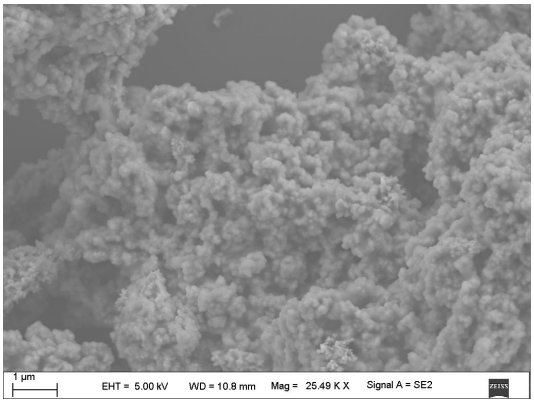

Figure S1. SEM image of PdNiP grain aggregates (GA).

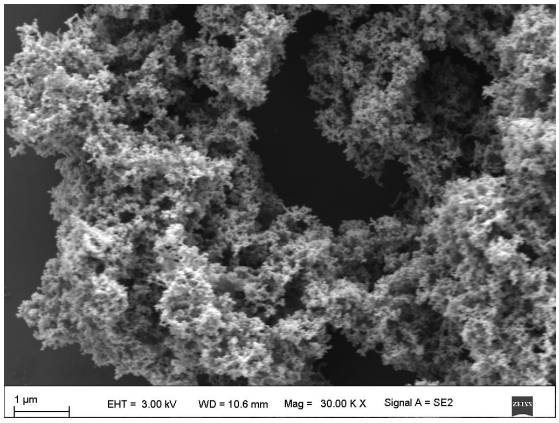

Figure S2. SEM image of the PdNiP NN prepared with Ar bubbles.

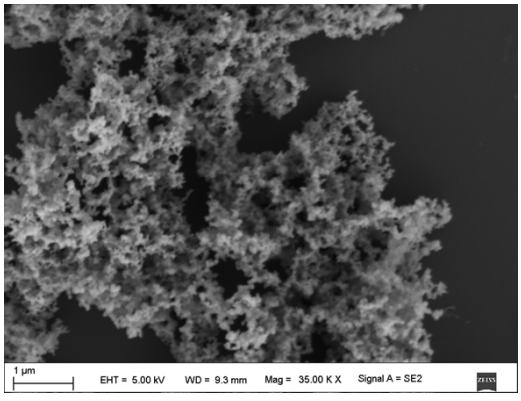

Figure S3. SEM image of the PdNi NN.

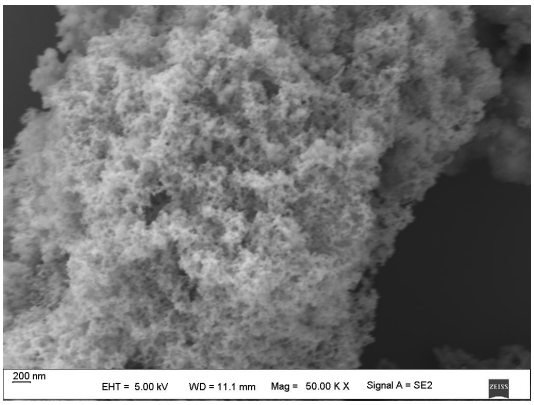

Figure S4. SEM image of the PdCoP NN.

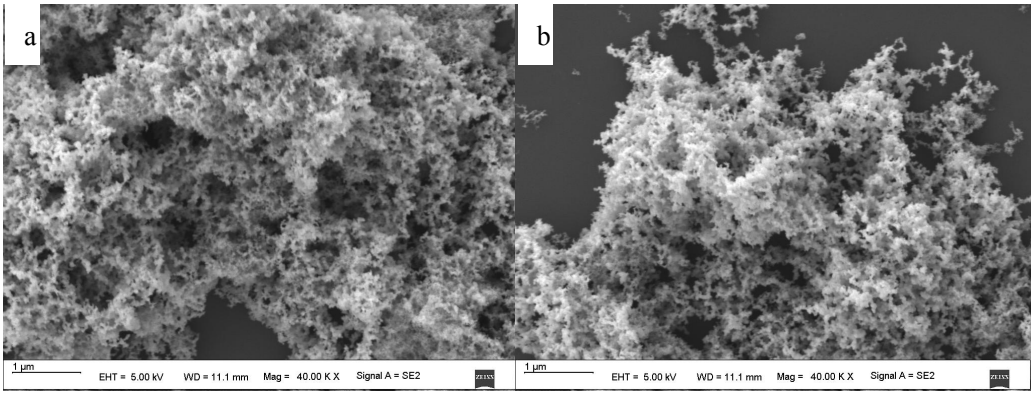

Figure S5. SEM images of PdNiP-2 (a) and PdNiP-3 (b) NN.

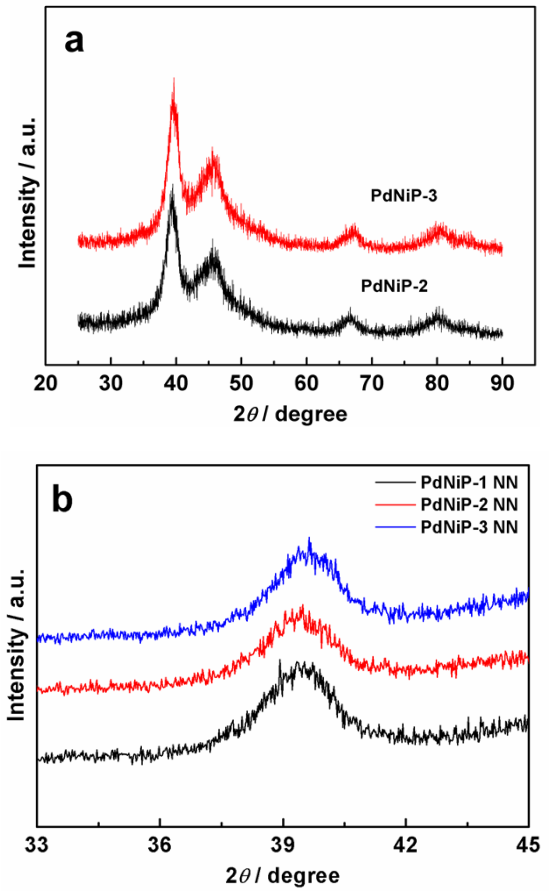

Figure S6. (a) XRD patterns of PdNiP-2 and PdNiP-3 NN, and (b) enlarged (111) peaks of PdNiP-1, PdNiP-2 and PdNiP-3 NN.

Figure S6 shows XRD patterns of PdNiP-2 and PdNiP-3 NN with four characteristic diffraction peaks of fcc Pd. Notably, no other peaks appeared, indicating the crystal structure was not influenced by changing the ratio of the precursors. To highlight the different crystal structure of PdNiP NN, the (111) diffraction peaks of PdNiP-1, PdNiP-2 and PdNiP-3 are enlarged into Figure S6b. The (111) peak shifted to the higher 2θ degree from PdNiP-1 to PdNiP-3, implying that the lattice parameter decreased. From Table S1, as the amount of added P was decreased, fewer and fewer P atoms incorporate into the PdNi lattice, leading to increasing smaller lattice parameter.

Table S2. Electrochemical performance of the five catalysts.

Sample	ECSA ($m^2g_{Pd}^{-1}$)	The onset potential for EOR (V)	The mass activity ($A\ mg^{-1}_{Pd}$)
PdNiP-1 NN	44.4	-0.706 vs. Hg/HgO	1.066 at -0.073 V
PdNiP-2 NN	51.1	-0.700 vs. Hg/HgO	1.219 at -0.045 V
PdNiP-3 NN	35.5	-0.657 vs. Hg/HgO	0.840 at -0.037 V
PdNi NN	18.9	-0.639 vs. Hg/HgO	0.367 at -0.116 V
PdNiP GA	3.5	-0.549 vs. Hg/HgO	0.183 at -0.126 V
PdNiP/C[17]	-	-0.61 vs. SCE	2.533
Pd_2Ni_1/C[18]	-	-0.58 vs. Hg/HgO	2.956
$Pd_{59}Ni_{41}$/C[19]	-	-0.56 vs. Ag/AgCl	0.44

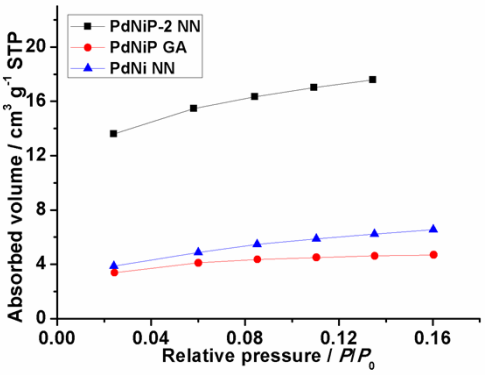

Figure S7. Nitrogen absorbed-isotherms of PdNiP-3 NN, PdNiP GA and and PdNi NN.

Table S3. BET surface area and C constant in three samples obtained from Figure S6.

Samples	BET surface area (m^2/g)	C constant
PdNiP-2 NN	67.2	379.6
PdNiP GA	17.7	252.8
PdNi NN	25.8	65.0

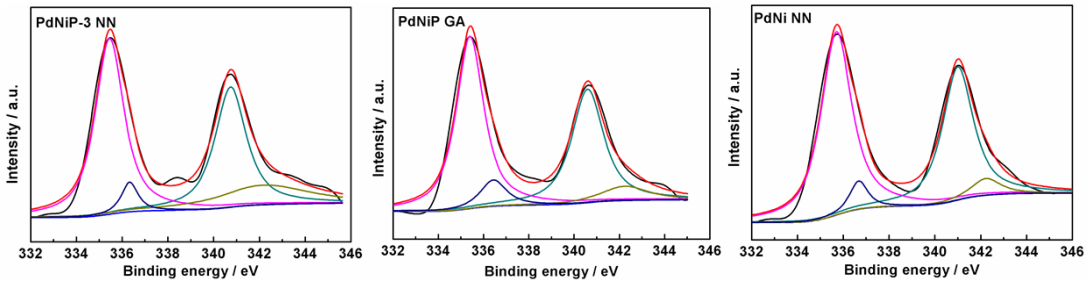

Figure S8. Pd 3d XPS spectra of PdNiP-3 NN, PdNiP GA and and PdNi NN.

Table S4. Assignments, Binding energies (BEs) and concentrations of Pd 3d species in three samples obtained from XPS results.

Samples	Pd 3d	BE[a]	Concentration[b]
PdNiP-3 NN	0	340.7&335.4	79.2
	2	342.2&336.3	20.8
PdNiP GA	0	340.6&336.4	86.0
	2	342.2&336.4	14.0
PdNi NN	0	341.0&335.7	90.7
	2	342.2&336.7	9.3

[a] Binding energy (in eV). [b] Per species (in at %).

XPS spectra of Pd 4d of the three catalysts are shown in Fig. S8. To identify different chemical states of Pd on the surface of the samples, the spectrum of Pd 3d XPS was fitted into two pairs of overlapping Lorentzian curves (see Table S4). Pd in the three catalysts is present in the zerovalent metallic and oxidation states. The binding energies of Pd 3d of PdNiP-2 and PdNiP GA shift negatively in comparison to that of PdNi, indicating that the electronic structures of PdNi were tuned by the introduction of P atoms because of the chemical interactions between Pd, Ni and P atoms.

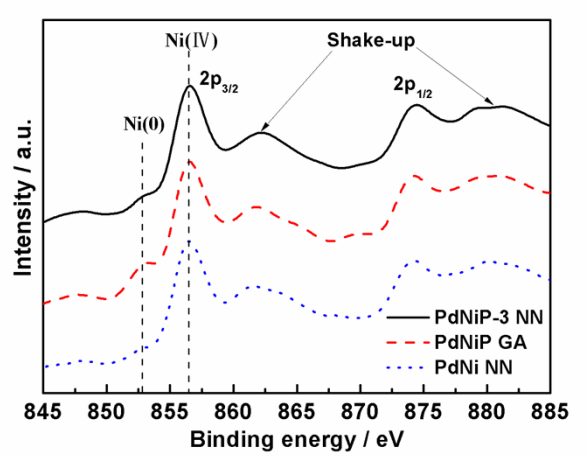

Figure S9. Ni 2p XPS spectra of PdNiP-3 NN, PdNiP GA and and PdNi NN.

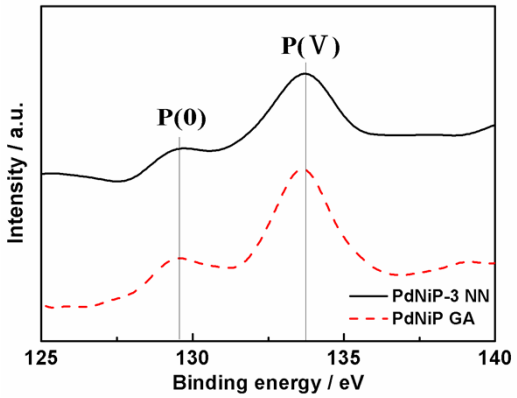

Figure S10. P 2p XPS spectra of PdNiP-3 NN, PdNiP GA and and PdNi NN.

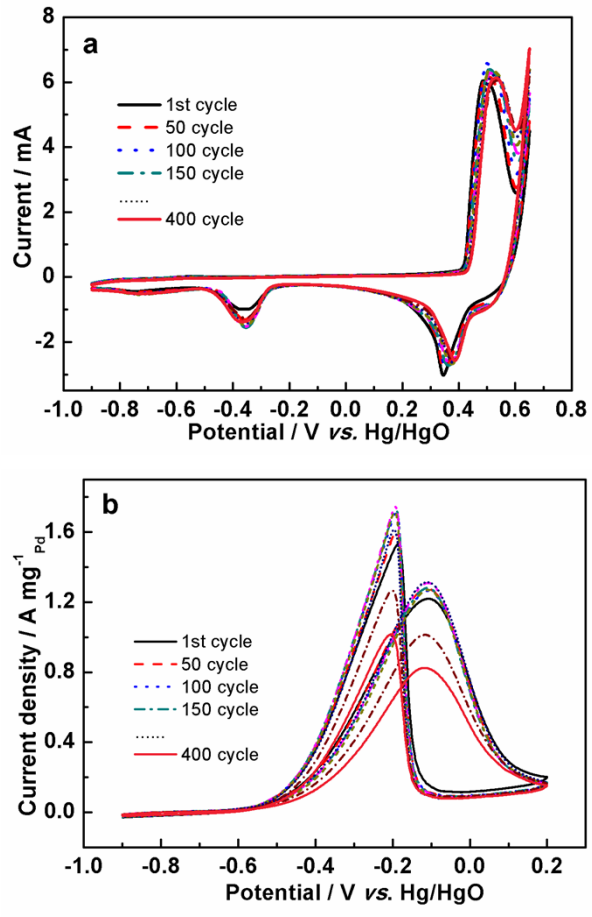

Figure S11. (a) CVs on PdNiP-2 NN electrode, Solution: N_2-saturated 1.0 mol L^{-1} KOH, scan rate: 50 mV s^{-1}. (b) EOR CVs on PdNiP-2 NN electrode at a scan rate of 50 mV s^{-1}; Solution: N_2-saturated 1.0 mol L^{-1} C_2H_5OH + 1.0 mol L^{-1} KOH.

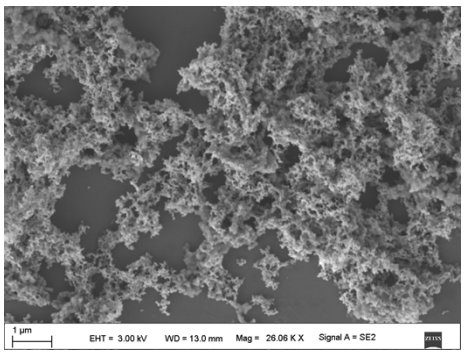

Figure S12. SEM image of PdNiP-2 NN after CV cycles. PdNiP-2 NN after CV cycles were collected following the process: after 400 cycles, the membrane on the electrode was dissolution into ethanol by ultrasonication. After dried in air, the sample was obtained.

The stability of PdNiP-2 NN was tested by CV cycles to evaluate their potential for practical applications. The CV cycles is following the process: CV cycles were firstly carried out in 1.0 mol L^{-1} KOH solution, the first, 50, 100, 150 …… 400 cycles were recorded with a scan rate of 50 mV s^{-1}, simultaneously, the first, 50, 100, 150 …… 400 cycles in 1.0 mol L^{-1} C_2H_5OH + 1.0 mol L^{-1} KOH were recorded with a scan rate of 50 mV s^{-1}. The obtained results were plotted in Fig. S11. After 400 cycles, the current of CV in KOH solution decreased in Fig. S11a, while EOR activity of PdNiP-2 NN in Fig. S11b exhibited significantly loss from 1.219 A mg^{-1}_{Pd} to 0.834 A mg^{-1}_{Pd}, in other words, PdNiP-2 NN loses nearly 31.6% of its mass activity after 400 cycles of potential cycling. Compared to the work of Zhang's group [Ref.6 in MS], the stability of PdNiP-2 NN is poor. To probe the origin of the loss of catalytic activity, SEM and XPS analysis were carried out. As shown in Fig. S12, the network structure of PdNiP-2 NN is retained, but the agglomeration occurs, resulting in the decrease of current in Fig. S11a. The composition of PdNiP-2 after the cycling test analyzed by ICP analysis is 1:4:1.8 of Pd:Ni:P molar ratio, indicating that Co and P, especially P, in the alkaline solution were leached, resulting in the agglomeration. Compared to the change of current in Fig. S11 a and b, the siginifcant decrease of catalytic activity was mainly ascribed to the leaching of P.